

27.9% Efficient Monolithic Perovskite/Silicon Tandem Solar Cells on Industry Compatible Bottom Cells

Eike Köhnen, Philipp Wagner, Felix Lang, Alexandros Cruz, Bor Li, Marcel Roß, Marko Jošt, Anna B. Morales-Vilches, Marko Topič, Martin Stolterfoht, Dieter Neher, Lars Korte, Bernd Rech, Rutger Schlatmann, Bernd Stannowski,* and Steve Albrecht*

Monolithic perovskite/silicon tandem solar cells recently surpass the efficiency of silicon single-junction solar cells. Most tandem cells utilize $>250\ \mu\text{m}$ thick, planarized float-zone (FZ) silicon, which is not compatible with commercial production using $<200\ \mu\text{m}$ thick Czochralski (CZ) silicon. The perovskite/silicon tandem cells based on industrially relevant $100\ \mu\text{m}$ thick CZ-silicon without mechanical planarization are demonstrated. The best power conversion efficiency (PCE) of 27.9% is only marginally below the 28.2% reference value obtained on the commonly used front-side polished FZ-Si, which are about three times thicker. With both wafer types showing the same median PCE of 27.8%, the thin CZ-Si-based devices are preferred for economic reasons. To investigate perspectives for improved current matching and, therefore, further efficiency improvement, optical simulations with planar and textured silicon have been conducted: the perovskite's bandgap needs to be increased by $\approx 0.02\ \text{eV}$ when reducing the silicon thickness from 280 to $100\ \mu\text{m}$. The need for bandgap enlargement has a strong impact on future tandem developments ensuring photostable compositions with lossless interfaces at bandgaps around or above 1.7 eV.


1. Introduction

Today's photovoltaic market is dominated by crystalline silicon-based solar cell technology. With a record power conversion efficiency (PCE) of 26.7%,^[1] silicon single-junction solar cells are approaching their theoretical limit of 29.4%.^[2] To overcome this limit, silicon solar cells can be combined with wider bandgap materials into multijunction solar cells, where each photovoltaic active material converts a specific part of the spectrum efficiently into electrical power. With two active materials (commonly termed tandem solar cells), the theoretical PCE limit is $\approx 46\%$ based on detailed balance arguments.^[3] The excellent optoelectronic properties as well as the tunable bandgap and potentially low-cost fabrication make metal halide perovskites suitable candidates for the top cell material in tandem solar cells.^[4–13] Only 3 years after the first realization of a p–i–n tandem solar cell by Bush et al.,^[14]

E. Köhnen, Dr. P. Wagner, B. Li, M. Roß, Dr. L. Korte, Prof. S. Albrecht
Helmholtz-Zentrum Berlin für Materialien und Energie GmbH
Young Investigator Group Perovskite Tandem Solar Cells
12489 Berlin, Germany
E-mail: steve.albrecht@helmholtz-berlin.de

Dr. F. Lang, Dr. M. Stolterfoht, Prof. D. Neher
Institute of Physics and Astronomy
University of Potsdam
14476 Potsdam, Germany

Dr. A. Cruz, Dr. A. B. Morales-Vilches, Prof. R. Schlatmann,
Prof. B. Stannowski
Helmholtz-Zentrum Berlin für Materialien und Energie GmbH
PVcomB
12489 Berlin, Germany
E-mail: bernd.stannowski@helmholtz-berlin.de

 The ORCID identification number(s) for the author(s) of this article can be found under <https://doi.org/10.1002/solr.202100244>.

© 2021 The Authors. Solar RRL published by Wiley-VCH GmbH. This is an open access article under the terms of the Creative Commons Attribution License, which permits use, distribution and reproduction in any medium, provided the original work is properly cited.

DOI: 10.1002/solr.202100244

Dr. M. Jošt, Prof. M. Topič
Faculty of Electrical Engineering
University of Ljubljana
Tržaška 25, 1000 Ljubljana, Slovenia

Prof. B. Rech
Helmholtz-Zentrum Berlin für Materialien und Energie GmbH
Scientific Management
12489 Berlin, Germany

Prof. B. Rech, Prof. S. Albrecht
Faculty IV – Electrical Engineering and Computer Science
Technical University Berlin
10587 Berlin, Germany

Prof. R. Schlatmann
Faculty 1 School of Engineering – Energy and Information
HTW Berlin–University of Applied Sciences
12459 Berlin, Germany

Prof. B. Stannowski
Faculty II – Mathematics, Physics, Chemistry
Beuth University of Applied Sciences Berlin
13353 Berlin, Germany

the highest scientifically reported efficiency of 29.15% is close to the theoretical limit of silicon single-junction solar cells.^[15] With a certified efficiency of 29.52%, Oxford PV surpassed this limit but did not disclose any further details.^[16]

These high efficiencies are achieved on rather thick front-side polished float-zone (FZ) silicon heterojunction solar cells, which are industrially not relevant for three reasons: 1) chemical–mechanical polishing (CMP) is time consuming and expensive. Therefore, it is desirable to use either chemical polishing as it is used in passivated emitter and rear cell (PERC) industry or double-side textured wafers. The latter approach is favored because such textures can be produced in a standard batch process and they provide optical advantages. Perovskite/silicon tandem processing on such wafers is addressed in recent publications.^[4,9,17–21] However, solution processing of high-efficiency tandem solar cells using such textures still remains challenging due to the difficulties of processing very thin perovskite layers on micrometer-sized pyramid structures. 2) FZ-silicon is not used for PV mass production. Instead, Czochralski (CZ) silicon will remain the main method to fabricate silicon ingots,^[22] mainly because of lower costs. 3) The absorption of Si for photon energies just above the bandgap, i.e., in the infrared (IR) part of the spectrum, is relatively poor. For tandem cells, however, where the top cell will absorb most of the higher energy photons, the IR response of the bottom cells is crucial.^[5,23] Therefore, the bottom cell thickness in most publications on perovskite/silicon tandem solar cells is 260 to 300 μm , whereas according to current market forecasts, the industrially relevant thickness for n-type monocrystalline silicon is just 140 to 150 μm (as cut) in 2022.^[24]

In this article, we demonstrate for the first time monolithic perovskite/silicon tandem solar cells based on thin non-CMP n-type CZ-silicon bottom cells. The reduced response in the IR region for thinner bottom cells will shift the optimal

top cell bandgap for standard test conditions toward larger energies.

2. Solar Cells

We use (100)-oriented $\approx 130 \mu\text{m}$ thick (as cut) n-type CZ-silicon wafers with random pyramids on the rear side and a specified resistivity of $\approx 5 \Omega \text{ cm}$. The front side of these CZ-based bottom cells was chemically polished using standard etching procedures in PERC industry but using a more aggressive treatment, removing up to 20 μm , to obtain a surface compatible with the top-cell processing.^[25,26] Tandem solar cells with these type of bottom cells are termed “CZ-based.” As a reference, we use (100)-oriented $280 \pm 20 \mu\text{m}$ thick FZ wafers with random pyramids on the rear side, a CMP front side, and a resistivity of $\approx 3 \Omega \text{ cm}$ (in the following termed “FZ-based”). The front and rear side of all wafers are passivated with intrinsic amorphous silicon ((i)a-Si:H) layers. On the rear side, p-doped a-Si:H is deposited on the passivating layer. N-doped nanocrystalline silicon oxide (nc-SiO_x:H) optimized in refractive index for optimum NIR incoupling on the front passivating layer serves as electron-selective contact.^[5] All silicon layers were deposited by plasma-enhanced chemical vapor deposition (PECVD). On top of the (n) nc-SiO_x:H layer, an In₂O₃-based transparent conducting oxide (TCO) is deposited, whereas the rear contact consists of a layer stack of aluminum-doped zinc oxide (AZO) and silver. More details can be found in the Materials and methods section in the Supporting Information. After processing the bottom cells, the measured thicknesses of the CZ- and FZ-based bottom cells are 100 and 280 μm , respectively. **Figure 1** shows photographs of the polished and nonpolished bottom cell front surfaces and the topography of the respective wafers acquired via confocal 3D laser scanning microscope (CLSM). For the CMP surface of the FZ silicon, horizontal artifacts appeared during acquisition

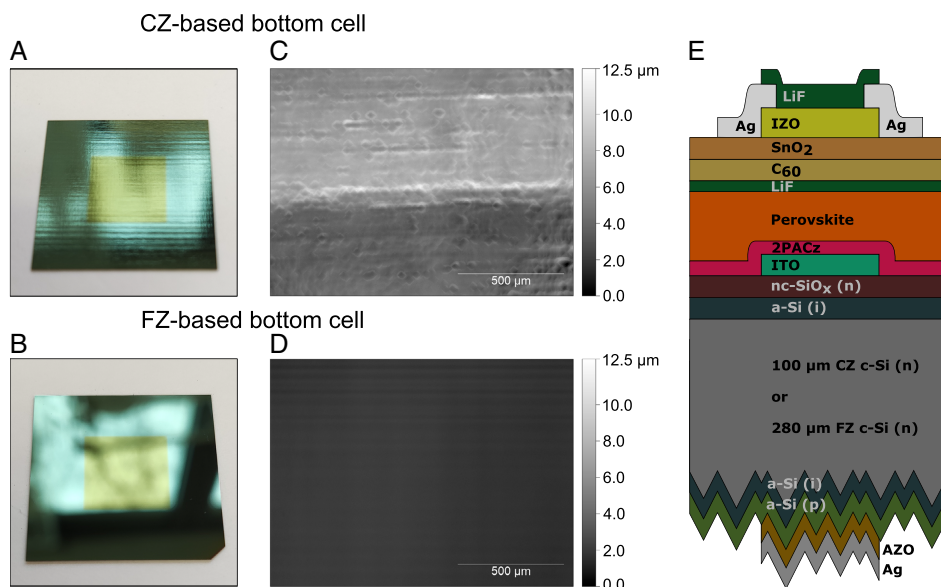


Figure 1. A, B) Photographs of the CZ-based silicon bottom cell and chemical–mechanical polished FZ-based silicon bottom cell. C, D) The topography of the CZ-based bottom cell and FZ-based bottom cell is acquired with a confocal laser scanning microscope and similar z-scalebars. E) Schematic stack of the monolithic perovskite/silicon tandem solar cell used in this work.

leading to falsified roughness values (see Figure S2, Supporting Information, for an adjusted scale). Therefore, atomic force microscopy (AFM) is used to image and analyze the surface of the FZ-based bottom cell (Figure S3, Supporting Information). The root mean square roughness values (S_q) are extracted from the areas as shown in Figure S3, Supporting Information. They amount to 1 and 736 nm for the FZ-based and CZ-based bottom cells, respectively. The maximum height values (S_z) are 9 nm and 7.7 μm for the FZ-based and CZ-based bottom cells, respectively. Although the S_z for CZ silicon is very high, the lateral dimension of the features is large enough to enable complete coverage during spin coating. This is evident for the saw mark visible for the CZ silicon in the CLSM image (Figure 1C): The step height is $\approx 5\text{--}6\ \mu\text{m}$ (see Figure S4, Supporting Information), but since it extends over 100 μm , it should not be problematic for solution-processed perovskite layers.

To investigate the influence of the different wafer types (i.e., thickness and topography) on the optical properties, we measured reflection of the bare wafers. The reflection spectra shown in Figure S5, Supporting Information, demonstrate that the reflection for wavelengths below 950 nm is not affected by the difference in topography or thickness. For longer wavelengths, the reflection is higher for the thin CZ silicon. Less light is absorbed due to the thinner silicon. Thus, the amount of light arriving at the rear side of the cell is increased, which consequently increases the amount of light reflected at the rear side, too. For the same reason, the light reflected at the rear side of the cell is absorbed less while being transferred back in the thinner silicon bottom cell, leading ultimately to an increased outcoupling at the front side and thus reflection.

For the p–i–n top cell which is identical on both types of bottom cells (Figure 1E), a self-assembled monolayer, 2PACz, is used as a hole-selective layer (HSL). In addition to its electrical advantages, it enables conformal coverage on the nonpolished bottom cell.^[27] The nominal perovskite composition is $\text{Cs}_{0.05}(\text{MA}_{0.23}\text{FA}_{0.77})_{0.95}\text{Pb}(\text{Br}_{0.23}\text{I}_{0.77})_3$ yielding a bandgap of 1.68 eV. On top of the perovskite, LiF and C_{60} are deposited via thermal evaporation and SnO_2 is deposited via atomic layer deposition. After the sputter deposition of zinc-doped indium

oxide (IZO) as transparent conductive oxide, Ag and LiF are thermally evaporated as split ring-type bus bar electrode and antireflective coating, respectively. The active area of the resultant tandem solar cells is 1 cm^2 . A detailed description can be found in the Materials and Methods section in the Supporting Information. To monitor the process, opaque perovskite single-junction solar cells with an active area of 0.16 cm^2 were fabricated together with the tandem solar cells. The median performance values (10 devices) for opaque perovskite single-junctions are 78.5% for the fill factor (FF), 20.3 mA cm^{-2} for the short-circuit current density (J_{SC}), 1.2 V for the open-circuit voltage (V_{OC}), and 19.3% for the PCE (see Figure S6, Supporting Information). A maximum efficiency of 19.9% with a V_{OC} of 1.21 V was obtained in this p–i–n type configuration, which is among the highest PCE and V_{OC} values for perovskite cells as typically used in two-terminal tandem solar cells.^[28]

Figure 2A shows the external quantum efficiency (EQE) and reflection spectra of two-terminal (monolithic) tandem solar cell champion devices based on thin CZ and thick FZ bottom cells. In the short-wavelength range, a minor difference in reflection occurs. We account this difference to very slight variations of layer thicknesses in the front contact, leading to altered interference patterns. The difference in the long wavelength range is a result of a difference in the bottom cell thickness, as described previously. For both tandem solar cells, the EQE spectra of the perovskite subcells (top cells) are very similar. Consequently, the photogenerated current densities (J_{ph}) under 100 mW cm^{-2} AM1.5 G illumination are also similar in both perovskite subcells (19.56 and 19.44 mA cm^{-2} for the CZ and FZ cells, respectively). The main difference between the tandem cells occurs in the EQEs of the silicon subcells (bottom cells). The J_{ph} in the silicon bottom cell of the thick FZ-based tandem solar cell is 19.08 mA cm^{-2} . The reduced bottom cell thickness in the CZ-based tandem solar cell causes a lower response in the near-IR region leading to a reduced photogenerated current density of 17.81 mA cm^{-2} . Therefore, the cumulative photogenerated current density decreases from ≈ 38.52 to $\approx 37.37\ \text{mA cm}^{-2}$. As the J_{SC} of tandem solar cells is mainly determined by the J_{ph} of the limiting subcell, a lower J_{SC} for the thin CZ-based tandem solar cell is expected. In contrast,

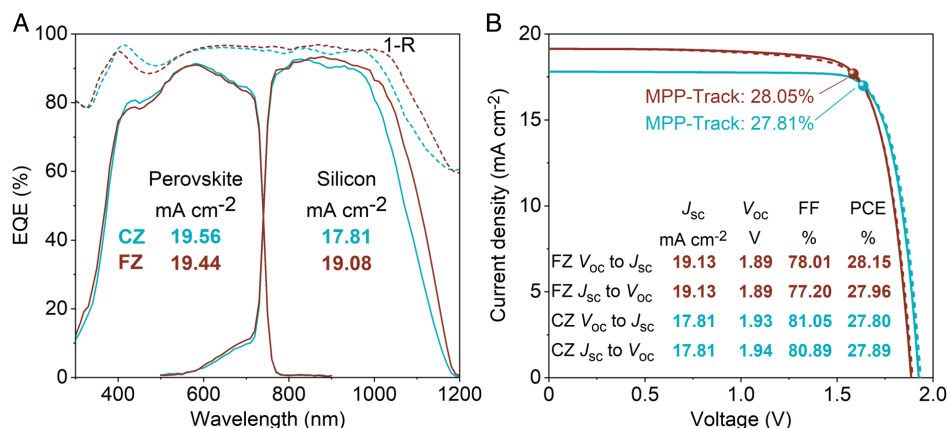


Figure 2. A) Comparison of the EQE spectra and reflection spectra (denoted as 1-R) between champion tandem solar cells based on thick FZ-silicon and thin CZ-silicon. B) J – V measurement of the tandem solar cells shown in (A) including the photovoltaic parameters and values obtained by 5 min MPP-tracking as shown in Figure S9, Supporting Information.

the current mismatch between the subcells increases. As we have reported previously, the tandem's FF is affected by the current mismatch.^[7] Generally, the FF increases with larger mismatch. In addition, thinner silicon wafers lead to higher V_{OC} values due to an decreasing total recombination current density.^[2] To estimate the gain in V_{OC} , we simulated silicon single-junction solar cells (illumination spectrum as in the tandem) with CZ- and FZ-silicon as used for tandem solar cells with the program Quokka3 (see Figure S7, Supporting Information, and the Materials and Methods section in the Supporting Information for more details). A V_{OC} enhancement of ≈ 17 mV is expected when using 100 μm CZ-silicon instead of 280 μm FZ-silicon. Even though the FF of the bottom cell also depends on the thickness and fabrication method, the simulations reveal that the configurations investigated in this work, both cell types, FZ and CZ, should deliver the same FF of 82.5% to 83% (see Figure S7, Supporting Information). Summarizing, the thinner CZ-based tandem solar cell is expected to have a lower J_{SC} , higher FF (due to larger current mismatch), and higher V_{OC} .

The J - V curves shown in Figure 2B confirm these expectations. The best reference device based on thick FZ wafers has a J_{SC} of 19.13 mA cm^{-2} , V_{OC} of 1.89 V, and FF up to 78.01% and as a result a PCE of up to 28.15%. This value is in very good agreement to our previous results for similar tandem layer stacks.^[15] For the thin CZ tandem solar cell, the high FF of 80.89% partially compensates the lower J_{SC} of 17.81 mA cm^{-2} . Combined with a higher V_{OC} of 1.94 V, the PCE of this cell is 27.89%. This value is just 0.26%_{abs} below the PCE of the front-side polished, thick FZ reference cell. Note that another J - V scan of the same cell led to a similar but yet slightly higher FF of 81.15% which is to the best of our knowledge the highest FF presented for perovskite/silicon tandem solar cells to date (see Figure S8, Supporting Information). The improvement of the FF per mismatch is higher than what we reported previously,^[7] but as elaborated by Boccard et al., the improvement in FF depends strongly on the performance of the individual subcells.^[29] Stable operation of the herein presented tandem solar cells is highlighted by 5 min maximum power point (MPP)-tracks as shown in Figure S9, Supporting Information. After 300 s MPP-tracking, PCE values of 28.05% and 27.81% are measured for the FZ- and CZ-based device, respectively, which is well in line with the J - V curve-derived efficiency. The illuminated J - V results for three CZ and four FZ tandem solar cells are summarized in Figure S10, Supporting Information. They reveal the same median PCE of 27.8% for both CZ- and FZ-based tandem solar cells. The V_{OC} improvement by 30 to 40 mV for the best devices is slightly more than expected from simulations. Therefore, we measured absolute photoluminescence of the top and bottom cell for both configurations to extract the quasi-Fermi level splitting (QFLS or implied V_{OC}).^[30,31] The intensity of the laser was set to match the current density generated within each subcell under AM1.5 G illumination. The PL spectra, QFLS values, and radiative limits are shown in Figure S11, Supporting Information. For the perovskite subcell, the QFLS values are the same on both the FZ- and CZ-based tandem solar cells. They amount to ≈ 1.20 eV, which is consistent with the V_{OC} of the perovskite single-junction solar cells (see Figure S6, Supporting Information). The QFLS of the silicon subcell in the FZ-based tandem solar cell is ≈ 690 meV.

Consequently, the sum of the perovskite and silicon QFLS for the FZ-based cell is ≈ 1.89 eV, which is in very good agreement with its V_{OC} extracted from the J - V curve (1.90–1.91 V for this specific sample). For the CZ-based tandem cell, a QFLS of 710 meV in the Si wafer was calculated. The enhancement of ≈ 19 meV compared to the FZ-based cell matches well with the simulated V_{OC} enhancement of 17 mV. We find well-agreeing values of the cumulative QFLS (1.910 eV) and the measured V_{OC} (1.92–1.93 V for this sample) for the CZ-based tandem cells. Therefore, we account the previously mentioned V_{OC} improvement of up to 40 mV to a sample to sample variation.

To exclude any structural changes in the perovskite due to different surface topographies of the bottom cells, X-ray diffraction (XRD) measurements were conducted. The XRD patterns acquired for the HSL/perovskite stack deposited on the different bottom cells reveal similar crystallization of the perovskite films on both surfaces (see Figure S12, Supporting Information). We attribute the additional peak around 32.8° for the FZ-sample to stem from the In_2O_3 -based recombination layer.

To analyze the effect of the bottom cell in more detail, we measured the J - V curve of the CZ-based tandem solar cell in a way that the J_{ph} values of both subcells are equal to the respective J_{ph} values in the FZ tandem solar cell (i.e., same mismatch conditions for CZ- and FZ-based tandem solar cells). This required to increase the illumination intensity only in the IR region of the spectrum, which can be easily done with the utilized light-emitting diode sunsimulator. In Figure S13, Supporting Information, this J - V measurement with adjusted J_{ph} values is compared to the J - V of the FZ tandem solar cell under AM1.5G conditions. In addition to the increased V_{OC} , just a slight deviation occurs at voltages just below the MPP. The FF values of both measurements are very similar, demonstrating that the increased FF of the CZ tandem solar cell under AM1.5G conditions arises mainly from the increased current mismatch.^[7]

The long-term stability of one CZ- and two FZ-based tandem solar cells (nonencapsulated) is shown in Figure S14, Supporting Information. The initial PCE values are 27.6% (CZ), 28.15% (FZ), and 27.4% (FZ). The cells were held at 25 °C in air, the relative humidity (RH) was not actively controlled. In addition to the J_{MPP} , V_{MPP} , the resulting PCE, and the normalized PCE, we show time series of the cell temperature and RH. The latter one ranges from 11% to 26%. After 1000 h continuous tracking, the cells were still performing at 67% (CZ), 70% (FZ), and 67% (FZ) of their respective initial PCE values, where the main parameter driving the reduction in PCE is J_{MPP} .

These efficient monolithic perovskite/silicon tandem solar cells demonstrate that it is not mandatory to use chemical-mechanical polishing for spin-coated perovskite films. Instead, chemical polishing as it is already deployed in industry, is sufficient for solution processing such as spin coating. Furthermore, it shows that industry relevant, almost threefold thinner CZ-silicon wafers can enable the same performance as the thick, CMP FZ-silicon wafers standardly used in lab-scale devices.

3. Optical Simulation

The reduced photogenerated current density for thinner silicon bottom cells necessitates adjustments to achieve current

matching or power matching conditions. Although the aforementioned experiment and previous reports demonstrate that the tandem solar cells are not highly sensitive to current mismatch conditions,^[7,32–34] the highest PCE values might be achieved with current or power matching conditions. Moreover, there are various effects affecting the mismatch conditions, as we will discuss later. Each of the effects needs to be controlled to obtain ultimately a current or power matched tandem solar cell.

Apart from increasing the IR response of the bottom cell by optical improvements, which is not the focus of this study, current matching can be achieved by reducing the perovskite thickness and/or widening the perovskite bandgap. To shed light on this aspect, we used GenPro4 to simulate the optical performance of tandem solar cells.^[35] We simulated tandem solar cells with a silicon bottom cell thickness of 100 and 280 μm . For both bottom cells, the perovskite thickness and its bandgap were varied. The lower limit of the thickness of 700 nm represents a realistic case as this thickness can be easily achieved with solution processing.^[9,10,17,18,21,36–38] As the J_{ph} saturates toward thicker films (Figure 3A), an upper limit of 1500 nm was chosen. For each thickness, the bandgap of the perovskite was varied by shifting the refractive index n and extinction coefficient k (measured via spectral ellipsometry for $E_g = 1.63$ eV) along the wavelength axis to cover a bandgap range of 1.63 to 1.78 eV (Figure S15, Supporting Information).^[39,40] The bandgap is taken as the inflection point of the perovskite absorption edge as shown in Figure S16, Supporting Information. All other layers were kept as in the experiment. An example of simulated EQE spectra with various perovskite bandgaps is shown in Figure S17, Supporting Information. Figure 3B shows the ideal top cell bandgap $E_{g,\text{top,matched}}$ as a function of the top cell's thickness when utilizing a 280 μm and 100 μm thick silicon bottom cell (see also Table S3, Supporting Information). The photogenerated current density of the perovskite top cell $J_{\text{ph,Perovskite}}$ increases with thicker perovskite layers. As a consequence, the photogenerated current density of

the silicon bottom cell $J_{\text{ph,Silicon}}$ decreases with thicker perovskite layers (Figure S18, Supporting Information). Thus, for thicker perovskite layers, it is necessary to widen the top cell bandgap if current matching is desired. When increasing the thickness from 700 to 1500 nm, the top cell bandgap needs to be increased by 0.047 eV for both bottom cell thicknesses. In the best case, this would improve the V_{OC} . As evident from Table S3, Supporting Information, the matched photogenerated current density $J_{\text{ph,matched}}$ stays almost constant. In addition, the bottom cell thickness alters current matching conditions. We found that the reduction of the bottom cell thickness from 280 to 100 μm requires to widen the top cell bandgap by 0.02 eV, regardless of the perovskite's thickness. However, simultaneously $J_{\text{ph,matched}}$ decreases from 19.64 to 19.14 mA cm^{-2} (average values). Therefore, for a perovskite thickness of 700 nm, its bandgap needs to increase from ≈ 1.69 to ≈ 1.71 eV if the bottom cell thickness is reduced. The higher V_{OC} from both top and bottom cell together (40–50 mV) will exactly compensate the reduced J_{SC} (when assuming that $J_{\text{ph,matched}} = J_{\text{SC}}$). Obviously, the FF of the perovskite top cells needs to remain the same regardless of the perovskite thickness to maintain the high PCE. Ultimately, a trade-off between high J_{SC} (thick silicon wafer and narrow perovskite bandgap) and high V_{OC} (thin silicon wafer and wide perovskite bandgap) needs to be made to yield the highest efficiency. Finding this optimum bottom cell thickness will be work for the future. These simulations do not include any optimization of other (e.g., contact) layer thicknesses. The adjustment of these layer thicknesses can reduce the interference patterns appearing, especially in the NIR wavelength range for the silicon subcell (see Figure S18, Supporting Information). This would require an optimization for each individual top cell bandgap and thickness.

The same simulations were performed for double-side textured tandem solar cells. As previously simulated and experimentally demonstrated,^[4,6,19,20] the additional front-side texture reduces reflection and removes interference patterns, enabling higher J_{ph} and J_{SC} values (see Figure S19, Supporting

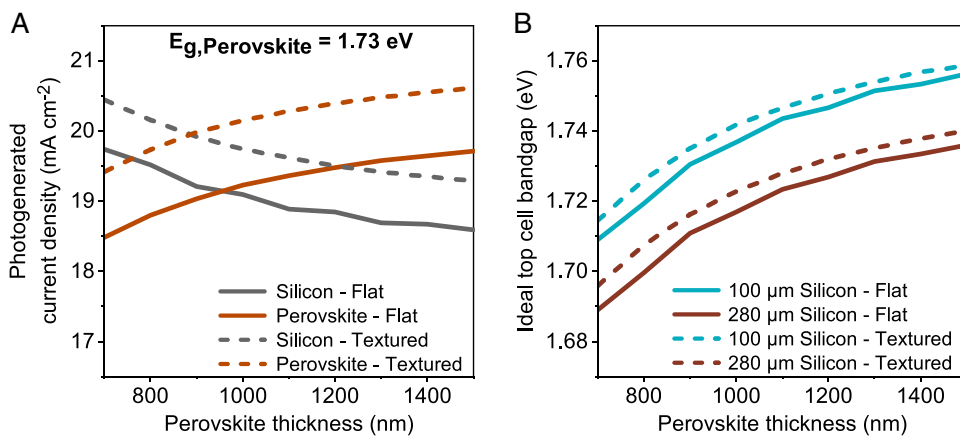


Figure 3. A) Simulated photogenerated current densities J_{ph} of perovskite/silicon tandem solar cells as a function of the perovskite thickness. The thickness of the silicon bottom cell is 100 μm and the perovskite bandgap is 1.73 eV. The rear side of the tandem cells is textured. The front side is either flat (denoted as “Flat”) or textured (denoted as “Textured”). The corresponding EQE spectra are shown in Figure S18, Supporting Information. B) Ideal top cell bandgap which is needed to obtain current matching conditions as a function of the perovskite's thickness. Reducing the thickness of silicon from 280 to 100 μm increases the ideal top cell bandgap by ≈ 0.02 eV for both textured and flat front sides. The values including the photogenerated current density are shown in Table S3 (Flat) and Table S4 (Textured), Supporting Information.

Information, for simulated EQEs). The same trends appear as for planar devices: With thinner silicon, a larger perovskite bandgap is needed to ensure current matching conditions (See Table S4, Supporting Information and Figure 3). When reducing the silicon thickness from 280 to 100 μm , the perovskite bandgap should increase by 0.019 eV to maintain current matching at the same perovskite thickness. However, this comes along with a reduction of $J_{\text{ph,matched}}$ by $\approx 0.5 \text{ mA cm}^{-2}$.

Ultimately, the optimum bandgap not just depends on the thickness of the perovskite layer and the thickness of the silicon wafer. Luminescence from the perovskite top cell into the silicon bottom cell will relax the requirement for current matching conditions.^[41] Furthermore, it was previously shown that higher operational temperatures and respective optical changes in top and bottom cells will lead to different optimum perovskite top cell bandgaps around 1.63 eV for highest energy yield with thick bottom cell wafers.^[20] The transition from a monofacial to a bifacial tandem solar cell reduces the bandgap as well, if current matching should be maintained.^[21] Therefore, the ideal device design cannot be easily derived from the performance under standard test conditions but needs to be derived for each case individually considering realistic outdoor conditions.

4. Conclusion

We demonstrated perovskite/silicon tandem solar cells based on industrially relevant silicon bottom cells, namely, 100 μm thin CZ-wafer with an industrial deployed chemical polishing for the front side and a textured rear side. For comparison, we fabricated tandem cells based on 280 μm thick FZ-wafers with a chemical–mechanical polished front side, which is standardly used in lab-scale devices. The CZ-based tandem cells have a PCE of up to 27.89%, which is just slightly below the value of 28.15% for FZ-based tandem cells. However, the median PCE of 27.8% indicates equal performance for both bottom cell types. The median V_{OC} increases from 1.89 V (max. 1.91 V) for the FZ-based cells to 1.92 V (max. 1.94 V) for the CZ-based cells, explained by the higher V_{OC} of the thin CZ bottom cell. Simultaneously, thinner silicon bottom cells present a lower EQE in the IR region, leading to a lower photogenerated current density and, thus, a lower J_{SC} (19.1 vs 17.8 mA cm^{-2}). The increased mismatch, when using an identical top cell, results in improved FF values (77.2% vs 80.9%). After 1000 h continuous MPP-tracking, the nonencapsulated cells still performed at 67% (CZ) and 67 to 70% (FZ) of their initial PCEs. We performed optical simulations to find current matching conditions for the 100 and 280 μm silicon bottom cells with planar and textured front sides. The perovskite bandgap needs to be increased by ≈ 0.02 eV when using a 100 μm thin silicon wafer instead of the commonly used thickness of 280 μm . Simultaneously, the expected J_{SC} reduces by $\approx 0.5 \text{ mA cm}^{-2}$. The higher V_{OC} from both top and bottom cell together (40 to 50 mV) can exactly compensate the reduction in J_{SC} for thinner wafers. Thus, to achieve highest PCE values with industrial bottom cells, the perovskite's bandgap needs to be widened to values well over 1.71 eV. The precise optimum top cell bandgap in this region is highly important, as these wide bandgap compositions are typically prone to phase segregation or are limited by nonradiative

recombination.^[42,43] Therefore, this work highlights that further investigation is needed to enable highly efficient and stable wider bandgap compositions and with that, highest tandem PCE values when using industry relevant bottom cells.

5. Experimental Section

Detailed information about the fabrication and characterization is given in the Supporting Information.

Supporting Information

Supporting Information is available from the Wiley Online Library or from the author.

Acknowledgements

The authors acknowledge help in technical assistance by T. Luřky, H. Heinz, M. Gabernig, and C. Ferber, Institute for Silicon Photovoltaics and M. Muske, T. Henschel, K. Mayer-Stillrich, H. Rhein J. Kleesiek, PVcomB. The authors acknowledge the support of Thorsten Dullweber and Silke Dorn (both ISFH) for the chemical polishing of CZ wafers. The authors acknowledge funding from HyPerCells (Hybrid Perovskite Solar Cells, <http://www.perovskites.de>) joint Graduate School, as well as from the German Federal Ministry for Economic Affairs and Energy (BMWi) through the "PersiST" project (grant no. 0324037C) as well as ProTandem (grant no. 0324288C). Further funding was provided by the Federal Ministry of Education and Research (BMBF) for funding of the Young Investigator Group Perovskite Tandem Solar Cells within the program "Materialforschung für die Energiewende" (grant no. 03SF0540) and by the Helmholtz Association within the projects HySPRINT Innovation lab and TAPAS (Tandem Perovskite and Silicon solar cells—Advanced optoelectrical characterization, modelling, and stability). F.L. acknowledges financial support from the Alexander von Humboldt Foundation via the Feodor Lynen program. The authors also acknowledge financial support by the Federal Ministry for Economic Affairs and Energy within the framework of the 7th Energy Research Programme (P3T-HOPE, grant no. 03EE1017C). M.J. and M.T. acknowledges financial support from the Slovenian Research Agency (ARRS) within the grants P2-0197 and J2-1727.

Open access funding enabled and organized by Projekt DEAL.

Conflict of Interest

The authors declare no conflict of interest.

Data Availability Statement

The data that supports the findings of this study are available in the supplementary material of this article or from the corresponding authors upon reasonable request.

Keywords

industry, perovskites, silicon, tandem solar cells

Received: April 2, 2021
Published online: May 5, 2021

- [1] K. Yoshikawa, H. Kawasaki, W. Yoshida, T. Irie, K. Konishi, K. Nakano, T. Uto, D. Adachi, M. Kanematsu, H. Uzu, K. Yamamoto, *Nat. Energy* **2017**, *2*, 17032.
- [2] A. Richter, M. Hermle, S. W. Glunz, *IEEE J. Photovoltaics* **2013**, *3*, 1184.
- [3] A. S. Brown, M. A. Green, *Phys. E: Low-Dimensional Syst. Nanostruct.* **2002**, *14*, 96.
- [4] F. Sahli, J. Werner, B. A. Kamino, M. Bräuninger, R. Monnard, B. Paviet-Salomon, L. Barraud, L. Ding, J. J. Diaz Leon, D. Sacchetto, G. Cattaneo, M. Despeisse, M. Boccard, S. Nicolay, Q. Jeangros, B. Niesen, C. Ballif, *Nat. Mater.* **2018**, *17*, 820.
- [5] L. Mazzarella, Y.-H. Lin, S. Kirner, A. B. Morales-Vilches, L. Korte, S. Albrecht, E. Crossland, B. Stannowski, C. Case, H. J. Snaith, R. Schlattmann, *Adv. Energy Mater.* **2019**, *9*, 1803241.
- [6] M. Jošt, E. Köhnen, A. B. Morales-Vilches, B. Lipovšek, K. Jäger, B. Macco, A. Al-Ashouri, J. Krč, L. Korte, B. Rech, R. Schlattmann, M. Topič, B. Stannowski, S. Albrecht, *Energy Environ. Sci.* **2018**, *11*, 3511.
- [7] E. Köhnen, M. Jošt, A. B. Morales-Vilches, P. Tockhorn, A. Al-Ashouri, B. Macco, L. Kegelmann, L. Korte, B. Rech, R. Schlattmann, B. Stannowski, S. Albrecht, *Sustain. Energy Fuels* **2019**, *3*, 1995.
- [8] B. Chen, Z. Yu, K. Liu, X. Zheng, Y. Liu, J. Shi, D. Spronk, P. N. Rudd, Z. Holman, J. Huang, *Joule* **2019**, *3*, 177.
- [9] Y. Hou, E. Aydin, M. De Bastiani, C. Xiao, F. H. Isikgor, D. Xue, B. Chen, H. Chen, B. Bahrami, A. H. Chowdhury, A. Johnston, S. Baek, Z. Huang, M. Wei, Y. Dong, J. Troughton, R. Jalmood, A. J. Mirabelli, T. G. Allen, E. Van Kerschaver, M. I. Saidaminov, D. Baran, Q. Qiao, K. Zhu, S. De Wolf, E. H. Sargent, *Science* **2020**, *367*, 1135.
- [10] J. Xu, C. C. Boyd, Z. J. Yu, A. F. Palmstrom, D. J. Witter, B. W. Larson, R. M. France, J. Werner, S. P. Harvey, E. J. Wolf, W. Weigand, S. Manzoor, M. F. A. M. van Hest, J. J. Berry, J. M. Luther, Z. C. Holman, M. D. McGehee, *Science* **2020**, *367*, 1097.
- [11] P. S. C. Schulze, A. J. Bett, M. Bivour, P. Caprioglio, F. M. Gerspacher, Ö. Ş. Kabaklı, A. Richter, M. Stolterfoht, Q. Zhang, D. Neher, M. Hermle, H. Hillebrecht, S. W. Glunz, J. C. Goldschmidt, *Sol. RRL* **2020**, *4*, 2000152.
- [12] D. Kim, H. J. Jung, I. J. Park, B. W. Larson, S. P. Dunfield, C. Xiao, J. Kim, J. Tong, P. Boonmongkolras, S. G. Ji, F. Zhang, S. R. Pae, M. Kim, S. B. Kang, V. Dravid, J. J. Berry, J. Y. Kim, K. Zhu, D. H. Kim, B. Efficient Shin, *Science* **2020**, *368*, 155.
- [13] M. Jošt, L. Kegelmann, L. Korte, S. Albrecht, *Adv. Energy Mater.* **2020**, *10*, 1904102.
- [14] K. A. Bush, A. F. Palmstrom, Z. J. Yu, M. Boccard, R. Cheacharoen, J. P. Mailoa, D. P. McMeekin, R. L. Z. Hoye, C. D. Bailie, T. Leijtens, I. M. Peters, M. C. Minichetti, N. Rolston, R. Prasanna, S. Sofia, D. Harwood, W. Ma, F. Moghadam, H. J. Snaith, T. Buonassisi, Z. C. Holman, S. F. Bent, M. D. McGehee, *Nat. Energy* **2017**, *2*, 17009.
- [15] A. Al-Ashouri, E. Köhnen, B. Li, A. Magomedov, H. Hempel, P. Caprioglio, J. A. Márquez, A. B. Morales Vilches, E. Kasparavicius, J. A. Smith, N. Phung, D. Menzel, M. Griseck, L. Kegelmann, D. Skroblin, C. Gollwitzer, T. Malinauskas, M. Jošt, G. Matič, B. Rech, R. Schlattmann, M. Topič, L. Korte, A. Abate, B. Stannowski, D. Neher, M. Stolterfoht, T. Unold, V. Getautis, S. Albrecht, *Science* **2020**, *370*, 1300.
- [16] National Renewable Energy Laboratory, Best Research-Cell Efficiency Chart, <https://www.nrel.gov/pv/cell-efficiency.html> (accessed: January 2021).
- [17] B. Chen, Z. J. Yu, S. Manzoor, S. Wang, W. Weigand, Z. Yu, G. Yang, Z. Ni, X. Dai, Z. C. Holman, J. Huang, *Joule* **2020**, *4*, 850.
- [18] A. S. Subbiah, F. H. Isikgor, C. T. Howells, M. De Bastiani, J. Liu, E. Aydin, F. Furlan, T. G. Allen, F. Xu, S. Zhumagali, S. Hoogland, E. H. Sargent, I. McCulloch, S. De Wolf, *ACS Energy Lett.* **2020**, *5*, 3034.
- [19] G. Nogay, F. Sahli, J. Werner, R. Monnard, M. Boccard, M. Despeisse, F.-J. Haug, Q. Jeangros, A. Ingenito, C. Ballif, *ACS Energy Lett.* **2019**, *4*, 844.
- [20] E. Aydin, T. G. Allen, M. De Bastiani, L. Xu, J. Ávila, M. Salvador, E. Van Kerschaver, S. De Wolf, *Nat. Energy* **2020**, *5*, 851.
- [21] M. De Bastiani, A. J. Mirabelli, Y. Hou, F. Gota, E. Aydin, T. G. Allen, J. Troughton, A. S. Subbiah, F. H. Isikgor, J. Liu, L. Xu, B. Chen, E. Van Kerschaver, D. Baran, B. Fraboni, M. F. Salvador, U. W. Paetzold, E. H. Sargent, S. De Wolf, *Nat. Energy* **2021**, *6*, 167.
- [22] International Technology Roadmap for Photovoltaic (ITRPV), 9th ed., <https://itrpv.vdma.org/documents/27094228/29066965/ITRPV0Ninth0-Edition02018.pdf/23bde665-600c-4f3f-c231-fed2568f08e0> (accessed: October 2019).
- [23] R. Santbergen, R. Mishima, T. Meguro, M. Hino, H. Uzu, J. Blaker, K. Yamamoto, M. Zeman, *Opt. Express* **2016**, *24*, A1288.
- [24] ITRPV. International Technology Roadmap for Photovoltaic (ITRPV), 11th ed., <https://itrpv.vdma.org/en/ueber-uns> (accessed: June 2020).
- [25] C. Kranz, S. Wyczanowski, U. Baumann, K. Weise, C. Klein, F. Delahaye, T. Dullweber, R. Brendel, *Energy Procedia* **2013**, *38*, 243.
- [26] C. Kranz, S. Wyczanowski, S. Dorn, K. Weise, C. Klein, K. Bothe, T. Dullweber, R. Brendel, in *27th European Photovoltaic Solar Energy Conf. and Exhibition*, Frankfurt, Germany **2012**, pp. 557–560.
- [27] A. Al-Ashouri, A. Magomedov, M. Roß, M. Jošt, M. Talaikis, G. Chistiakova, T. Bertram, J. A. Márquez, E. Köhnen, E. Kasparavicius, S. Levenco, L. Gil-Escrig, C. J. Hages, R. Schlattmann, B. Rech, T. Malinauskas, T. Unold, C. A. Kaufmann, L. Korte, G. Niaura, V. Getautis, S. Albrecht, *Energy Environ. Sci.* **2019**, *12*, 3356.
- [28] J. Tong, Q. Jiang, F. Zhang, S. B. Kang, D. H. Kim, K. Zhu, *ACS Energy Lett.* **2021**, *6*, 232.
- [29] M. Boccard, C. Ballif, *ACS Energy Lett.* **2020**, *5*, 1077.
- [30] M. Jošt, T. Bertram, D. Koushik, J. A. J. A. Marquez, M. A. M. A. Verheijen, M. D. M. D. Heinemann, E. Köhnen, A. Al-Ashouri, S. Braunger, F. Lang, B. Rech, T. Unold, M. Creatore, I. Lauermann, C. A. C. A. Kaufmann, R. Schlattmann, S. Albrecht, *ACS Energy Lett.* **2019**, *4*, 583.
- [31] M. Stolterfoht, C. M. Wolff, J. A. Márquez, S. Zhang, C. J. Hages, D. Rothhardt, S. Albrecht, P. L. Burn, P. Meredith, T. Unold, D. Neher, *Nat. Energy* **2018**, *3*, 847.
- [32] M. Meusel, R. Adelhelm, F. Dimroth, A. W. Bett, W. Warta, *Prog. Photovoltaics Res. Appl.* **2002**, *10*, 243.
- [33] W. E. McMahon, K. E. Emery, D. J. Friedman, L. Ottoson, M. S. Young, J. S. Ward, C. M. Kramer, A. Duda, S. Kurtz, *Prog. Photovoltaics Res. Appl.* **2008**, *16*, 213.
- [34] C. Ulbrich, C. Zahren, A. Gerber, B. Blank, T. Merdzhanova, A. Gordijn, U. Rau, *Int. J. Photoenergy* **2013**, *2013*, 1.
- [35] R. Santbergen, T. Meguro, T. Suezaki, G. Koizumi, K. Yamamoto, M. Zeman, *IEEE J. Photovoltaics* **2017**, *7*, 919.
- [36] B. Chen, S. Baek, Y. Hou, E. Aydin, M. De Bastiani, B. Scheffel, A. Proppe, Z. Huang, M. Wei, Y. Wang, E. Jung, T. G. Allen, E. Van Kerschaver, F. P. García de Arquer, M. I. Saidaminov, S. Hoogland, S. De Wolf, E. H. Sargent, *Nat. Commun.* **2020**, *11*, 1257.
- [37] F. Xu, J. Liu, A. S. Subbiah, W. Liu, J. Kang, G. T. Harrison, X. Yang, F. H. Isikgor, E. Aydin, M. De Bastiani, S. De Wolf, *Small Sci.* **2021**, *2000044*.
- [38] A. Y. Alsalloum, B. Turedi, K. Almasabi, X. Zheng, R. Naphade, S. D. Stranks, O. F. Mohammed, O. M. Bakr, *Energy Environ. Sci.* **2021**, *14*, 2263.
- [39] S. Albrecht, M. Saliba, J.-P. Correa-Baena, K. Jäger, L. Korte, A. Hagfeldt, M. Grätzel, B. Rech, *J. Opt.* **2016**, *18*, 064012.

- [40] K. Jäger, L. Korte, B. Rech, S. Albrecht, *Opt. Express* **2017**, 25, A473.
- [41] A. R. Bowman, F. Lang, Y. Chiang, A. Jiménez-Solano, K. Frohna, G. E. Eperon, E. Ruggeri, M. Abdi-Jalebi, M. Anaya, B. V. Lotsch, S. D. Stranks, *ACS Energy Lett.* **2021**, 6, 612.
- [42] E. T. Hoke, D. J. Slotcavage, E. R. Dohner, A. R. Bowring, H. I. Karunadasa, M. D. McGehee, *Chem. Sci.* **2015**, 6, 613.
- [43] F. Peña-Camargo, P. Caprioglio, F. Zu, E. Gutierrez-Partida, C. M. Wolff, K. Brinkmann, S. Albrecht, T. Riedl, N. Koch, D. Neher, M. Stolterfoht, *ACS Energy Lett.* **2020**, 5, 2728.